RSC Advances

This is an *Accepted Manuscript*, which has been through the Royal Society of Chemistry peer review process and has been accepted for publication.

Accepted Manuscripts are published online shortly after acceptance, before technical editing, formatting and proof reading. Using this free service, authors can make their results available to the community, in citable form, before we publish the edited article. This *Accepted Manuscript* will be replaced by the edited, formatted and paginated article as soon as this is available.

You can find more information about *Accepted Manuscripts* in the **Information for Authors**.

ROYAL SOCIETY OF CHEMISTRY

www.rsc.org/advances

Shape Memory Copolymer based on 2-(Dimethylamino) Ethyl Methacrylate and Methyl Allyl Polyethenoxy Ether for Potential Biological Applications

Yangyang, Chen[&a], Funian Mo[&a], Shaojun Chen[a], Yan Yang[a], Shiguo Chen[a]，Haitao Zhuo*[b], Jianhong Liu[b]；*

This study reports a novel shape memory copolymer synthesized with 2-(dimethylamino)-ethyl-methacrylate (DMAEMA) and methyl-allyl-polyethenoxy-ether (TPEG) for potential biological applications. In the DMAEMA-TPEG copolymers, TPEG segments form a semi-crystalline phase that serves as the reversible phase, while DMAEMA segments form an amorphous phase containing physical interactive networks that serve as the hard phase. As the TPEG content increases, crystallinity and the rate of crystallization increase, and the TPEG phase changes from dispersed small spherical crystals to a continuous crystalline phase. Additionally, good crystallinity of the TPEG phase endows the copolymers with good shape fixity, whereas the shape recovery decreases as the TPEG content decreases. DMAEMA-TPEG copolymers also exhibit the multi-shape memory effect with a good triple-shape memory effect. Finally, the investigation of the water contact angle illustrates that all DMAEMA-TPEG copolymers have good hydrophilicity. Thus, it is proposed that DMAEMA-TPEG copolymers might have great potential for biological applications.

Keywords: Shape Memory; Biomaterials; Polyethylene Glycol; Biological Applications; Polyampholytes;

Introduction

Shape memory polymers are materials that can memorize temporary shapes and revert to their permanent shape upon exposure to an external stimulus such as heat, light and moisture[1]. To achieve shape memory effect, polymers are generally designed and synthesized to form micro-phase separation structure consisting of soft phase (or reversible phase) and hard phase (or fixed phase). Therefore, many kinds of segmented copolymers have been synthesized successfully by free radical polymerization method for shape memory applications[2]. The

1

reported shape memory copolymers include poly-3-hydroxyalkanoates-co-polyethylene glycol methacrylate copolymers,[3] poly(acrylamide-co-acrylic acid),[4] poly(stearyl acrylate-co-acrylamide),[5] and poly(octadecyl acrylate-b-styrene-b-octadecyl acrylate).[6] Most of the reported shape memory copolymers show dual-shape memory effect which can just memorize one temporary shape. Recently, multi-shape memory polymers capable of memorizing more than two temporary shapes have received much attention of researcher. The multi-shape memory polymer should remarkably widen the range of applications of shape memory polymers in future. Copolymerization provides a facile way to fabricate more and more copolymers exhibiting multi-shape memory effect.

In addition, polymers containing ionic groups ranging from naturally occurring biopolymers to synthetic viscosifiers and soaps have also received significant attention from researchers. Particularly, zwitterionic polymers containing both cationic and anionic groups have found many promising applications in hemodiafiltration,[7] antifouling surfaces,[8] tumour therapy,[9] gene delivery and bioimaging.[10] In addition to the zwitterionic polymers synthesized with zwitterionic moieties, such as ammoniophosphates, ammoniosulfonates, ammoniocarboxylates and pyridicarboxylates,[11] many types of polyampholytes can be also synthesized from conventional functional monomers followed by further ionization.[12] 2-(Dimethylamino) ethyl methacrylate (DMAEMA) is a typical functional monomer for synthesis of polyampholytes and polyzwitterions.[12] For example, DMAEMA was copolymerized with N-(3-(methacryloylamino) propyl)-N, N-dimethyl-N-(3-sulfopropyl) ammonium hydroxide for serum-resistant gene delivery and bioimaging.[10] Biomimetic core cross-linked nano-carriers were constructed from a DMAEMA copolymer with carboxybetaine and styrene for the controlled release of bioactive agents.[13] Dihydroxy-terminated DMAEMA was also synthesized to prepare zwitterionic polyurethane for protein resistance.[14, 15] There are also many reports about the DMAEMA copolymers with 2-(diethylamino)ethyl methacrylate,[16] 2-(N-morpholino) ethyl methacrylate,[17] butyl methacrylate,[18] oligo(ethylene glycol) methyl ether methacrylate,[19] and methacrylic acid.[20] DMAEMA copolymers not only have great potential biomedical applications, but also can be further betainized to zwitterionic polymers with many biological functionalities, including high resistance to non-specific protein adsorption, antimicrobial, noncytotoxic, biocompatible

and biomimetic properties.[21-24]

Polyethylene glycol (PEG) is another attractive monomer for various biomaterials due to its low cytotoxicity, good biocompatibility and good hydrophilicity.[25, 26] Over the past decades, PEG-based polymers have been widely proposed for ultralow fouling coating,[27] cancer therapy,[28-30] implantable scaffolds,[31, 32] drug delivery,[33] cellular nucleic acid delivery[34] and tissue engineering.[35, 36] These great applications also encourage the development of new functional PEG derivatives, such as poly(ethylene glycol) methyl ether methacrylate,[37, 38] poly(ethylene glycol) monomethyl ether,[39] poly(propylene glycol methacrylate),[40, 41] and di(ethylene glycol) methyl ether methacrylate.[42] Recently, to achieve better biocompatibility, a diverse range of DMAEMA copolymers with PEG has been rapidly developed for various biomedical applications. For example, redox-cleavable miktoarm star polymers have been proposed as drug delivery carriers.[37] Stimuli-responsive imaging agents have been proposed for detection of the acidic environment within tumour tissues.[38] Multifunctional triblock copolymers have been designed to enhance the intracellular messenger RNA delivery.[43] Amphiphilic diblock copolymers were constructed for potential applications spanning drug and gene delivery, blood compatible coatings and aqueous lubrication.[44] Additionally, PEGylated polycaprolactone nanoparticles grafted with DMAEMA were also designed to improve the gene silencing efficiency of siRNA.[45] PEG and PEG derivatives have also been widely used to design shape memory polymers for smart biomedical applications.[46-49] In the previous literatures, shape memory copolymers synthesized from PEG and poly(epsilon-caprolactone) (PCL) have been proposed for dual drug-eluting biodegradable stents,[50] tissue engineering scaffolds and minimally invasive medical devices.[51] Shape memory gels synthesized in the presence of a PEG-based crosslinker have been proposed for a potential cell-encapsulating tubular scaffold application.[52] Many reports also exist about shape memory copolymers based on functional PEG derivatives, such as PEG methacrylate,[3] PEG diacrylates,[46] and PEG dimethacrylate.[53] However, to date, there are no reports of shape memory copolymers derived from methyl allyl polyethenoxy ether (TPEG) containing both PEG segment and vinyl group.

The objective of this study is to develop a new type of copolymer with TPEG and DMAEMA for shape memory biological applications because both TPEG and DMAEMA

3

segments generally have good biocompatibility. DMAEMA-TPEG shape memory copolymers, coded as p(DMAEMA-co-TPEG)**,** are expected to show good biocompatibility and good hydrophilic properties. In addition to the synthesis of p(DMAEMA-co-TPEG), the structure, morphology, thermal, hydrophilic, dynamic mechanical and shape memory properties are carefully investigated in this study. Additionally, the isothermal crystallization kinetics for the TPEG soft phase is studied because of its good crystallization and interesting sphere crystalline morphology.

Experimental Section

Materials

Methyl ally polyethenoxy ether (M_n=2400g/mol, TPEG2400) was purchased from Shandong-Bok Chemical Co. Ltd. (Shandong, China). Ammonium persulphate ($NH_4S_2O_8$), 2-(dimethylamino) ethyl methacrylate (DMAEMA), and other chemicals were purchased from Aladdin (Shanghai, China).

Synthesis of p(DMAEMA-co-TPEG)

Table 1. Composition of synthesized p(DMAEMA-co-TPEG)

Sample	Elemental composition (wt.%)				Content in copolymer (wt.%) calculated by EA*		Molecular weight ($\times 10^4$ g/mol) by GPC[#]	
	N	C	H	S	TPEG	DMAEMA	M_n	M_W
TPEG20	6.21	57.07	9.23	0.19	30.27	69.73	-	-
TPEG30	5.26	26.11	9.15	0.19	40.93	59.07	-	-
TPEG40	4.63	56.20	9.13	0.17	48.00	52.00	-	-
TPEG50	4.17	55.67	9.08	0.22	53.17	46.83	1.90	1.92
TPEG60	2.93	54.39	9.02	0.19	67.10	32.90	1.93	1.94
TPEG80	1.41	51.80	9.31	0.23	84.17	15.83	1.91	1.93

*EA: Elemental Analyzer on basis of the N weight. # GPC was conducted with DMF eluent, but TPEG20, TPEG30 and TPEG40 cannot be dissolved in DMF.

A series of p(DMAEMA-co-TPEG) with different TPEG contents was synthesized by adjusting the DMAEMA/TPEG weight ratio (**Table 1**). The synthetic route is presented in **Scheme 1**. The preparation was performed in a nitrogen filled and mechanically stirred 500-ml three-neck flask. After the functional monomers, DMAEMA and TPEG, were added

to the flask, polymerization was initiated by the addition of 5 mM ammonium persulphate in a monomer water solution, which proceeded at 60℃ for 10 hours (h) under constant stirring. Finally, the water was evaporated from the resulting 20 wt.% polymer solution in a Teflon pan at 80℃ for 24 h in a continuous air flow and then *in vacuum* for another 24 h. In this study, the names of the p(DMAEMA-co-TPEG) samples were coded as TPEG#, in which "#" refers to the TPEG weight percentage in the feed, e.g., TPEG20.

Scheme 1. Polymerization reaction of p(DMAEMA-co-TPEG)

Material Characterizations

ATR-FTIR spectra were scanned from smooth polymer films with a thickness of 0.2 mm using a Nicolet 760 FT-IR spectrometer by the FT-IR attenuated total reflection (ATR) method. Ten scans at a 4 cm^{-1} resolution were signal-averaged and stored as data files for further analysis.

The weight percentages of C, H, N and S of the samples were determined using a Vario EL III elemental analyser (Germany Elementar, Germany).

The molecular weight of copolymers was determined by GPC (Waters e2695, USA) using DMF as the eluent at 25℃ temperature.

The ^{1}H-NMR spectrum was recorded with an Avance-400Hz instrument (Bruker, Germany) using D_2O as the solvent.

DSC curves were determined using a TA-Q200 instrument with nitrogen purge gas. Indium and zinc standards were used for calibration. Samples were first heated from -60℃ to 150℃ at a heating rate of 10°C/min and maintained at 150℃ for 1 min, then they were

cooled to -60℃ at a cooling rate of 10°C/min, and finally, a second heating scan from -60℃ to 150℃ with 10°C/min was recorded for analysis.

TGA curves were recorded on a computer-controlled TA TG Q50 system (TA, America) under the following operational conditions: heating rate of 10℃/min to a final temperature of 600℃, sample weight of approximately 5.0 mg, using the film sample in platinum crucibles, a 60 ml/min N_2 flow. Three or four repeated readings (temperature and weight loss) were performed on the same TG curve, each having at least 15 points.

Dynamic-mechanical analysis (DMA) was determined using a TA Q200 instrument (TA, America) purged with nitrogen at ν=1 Hz at a heating rate of 2°C/min from -60 to 180°C. Specimens for DMA testing were prepared by film casting with a thickness of 0.5 mm, a width of 5 mm, and a length of 25 mm.

Nanonavi E-Sweep (SII Nanotechnology Inc., Germany) atomic force microscopy (AFM) was used in the tapping mode for morphological characterization of the dried sample. The samples were dissolved in water at a concentration of 5 mg/ml and spin-coated at 400 rpm for 10 s and then at 4000 rpm for 60 s on oxidised silicon substrates. The spin-coated films were placed in a 50 ℃ oven for 48 h to evaporate the solvent.

Static contact angle measurements were performed on a JC2000Y stable contact angle analyser (Chengde Chengwei Tester Co. Ltd. China) at room temperature with distilled water as the test liquid. For each sample, the measurements were repeated at three different locations of the sample.

The thermal-induced shape memory behaviours were determined with thermo-mechanical analysis using a DMA800 instrument (tension clamp, controlled force mode) according to the procedure described in the literature[54]. The detailed test setup for the dual-shape memory cycles, triple-shape memory cycles and multi-staged shape recovery cycles are provided in the supporting information **(Test S1)**. Shape fixity and shape recovery were used to characterize the effectiveness of fixing a temporary shape and the effectiveness of the shape recovery in each step; the detailed calculations are provided in the supporting information **(Test S1)**.

Characterization for isothermal crystallization kinetics

Isothermal crystallization experiments were performed with a TA-Q200 DSC instrument

using nitrogen as the purge gas. The sample (4–6 mg) was initially heated to 70℃ at a rate of 10℃/min and held for 5 min to remove the thermal history of the crystallizable phase. Subsequently, the sample was rapidly cooled (60℃/min) to a designated crystallization temperature (T_c) and held at this temperature until the end of the exothermic crystallization. The heat flow during the isothermal crystallization process was recorded as a function of time. T_c was chosen as 30℃ in this experiment. The amounts of heat generated during the development of the crystal phase were recorded and analyzed according to the typical equation used for evaluating the relative degree of crystallinity (X_t)[55]:

$$X_t = \frac{\int_{t0}^{t}\left(\frac{dH}{dt}\right)dt}{\int_{t0}^{t=\infty}\left(\frac{dH}{dt}\right)dt} \tag{1}$$

where t_0 and t=∞ are the time at which the sample reaches isothermal conditions (as indicated by a flat baseline after an initial spike in the thermal curve) and the time at which the dominant sharp exothermic peak ends, respectively. H is the enthalpy of crystallization at time t. After isothermal crystallization, the sample was heated to 100℃, and T_m, indicated by the maximum of the endothermic peak, was recorded.

The crystallization kinetics were analyzed with the modified Avrami equation, called the Ozawa equation[55]:

$$X(t) = 1 - \exp(-Kt^n) \tag{2}$$

Equation (2) can be converted into the following form:

$$\log\{-\ln[1 - X(t)]\} = n\log t + \log K \tag{3}$$

A plot of $\log\{-\ln[1-X(t)]\}$ against $\log t$ should yield a straight line. By fitting the lines, n and $\log K$ could be calculated from the slope and intercept, respectively.

Additionally, the half-crystallization time [t(0.5)] is defined as the time at which the crystallinity is equal to 50%, and it is related to the Avrami parameter K as determined with the following expression:

$$K = \ln 2 / [t(0.5)]^n \tag{4}$$

Results and Discussion

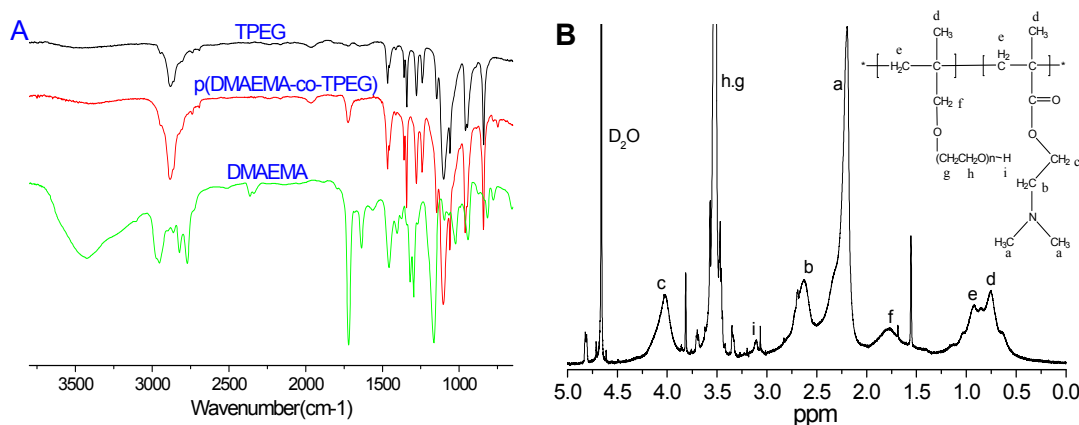**Molecular Structure Analysis**

Figure 1. Molecular structure analysis of p(DMAEMA-co-TPEG): (A-ATR-FTIR spectra of p(DMAEMA-co-TPEG) compared with TPEG, DMAEMA; B-^{1}H-NMR spectrum of sample TPEG50)

The molecular structure of p(DMAEMA-co-TPEG) is carefully investigated with elementary analysis (**Table 1**), ATR-FTIR and ^{1}H-NMR (**Figure 1**). The FT-IR spectrum of TPEG shows no frequency of C=O, implying the different molecular structure of TPEG from the traditional PEG derivatives based on methacrylate.[37-42] The vibration frequency of C=C appears at approximately 1640 cm^{-1} in DMAEMA but disappears after polymerization with TPEG in sample TPEG50, implying the successful polymerization of DMAEMA by the free-radical polymerization method. The C=O frequency at 1721 cm^{-1} and the C-O-C frequency at 1104-1146 cm^{-1} are detected in sample TPEG50, suggesting the successful copolymerization of DMAEMA with TPEG (**Figure 1A**).[56] Additionally, by adjusting the TPEG content, the frequencies of the C=O and C-O-C groups only slightly change (**Figure S1**), suggesting the successful preparation of p(DMAEMA-co-TPEG) with various TPEG contents. The ^{1}H-NMR spectrum of sample TPEG50 shows that the signal at 2.19 ppm is assigned to the methyl protons next to the nitrogen atom ($-N(CH_3)_2$, a) of the DMAEMA units. The peak at 2.63 ppm is attributed to the methylene protons on the DMAEMA units ($-CH_2-N(CH_3)_2$, b). The peak at 4.03 ppm is resulted from another methylene protons （$-O-CH_2-$, c）on the DMAEMA units. The protons of methyl ($-CH_3$, d) and methylene ($-CH_2-$, e) on the backbone are detected at 0.5∼1.0ppm.[44] The protons of methylene ($-CH_2-O$,

8

f) from the TPEG unit can only be detected at 1.5 ∼ 2.0ppm. Additionally, the chemical shift

at 3.52 ppm is attributed to the methylene protons on the PEG units (-O-CH$_2$-CH$_2$-O-, g, h),

and the signal appearing at 3.11 ppm represents the protons at the end group (-OH, i) (**Figure**

1B).[57] This information further confirms the successful copolymerization of DMAEMA with

TPEG. Additionally, the elementary analysis (EA) detects the existence of N, O, H and S,

which are from the residue of ammonium persulphate. The TPEG content calculated based on

the N weight tends to be higher than that in the feed, implying the presence of residues of

unreacted TPEG. However, as the TPEG content increases, the N content linearly decreases

due to the decrease of DMAEMA content. This result confirms that the DMAEMA-TPEG

copolymers with various TPEG contents are successfully prepared from DMAEMA and

TPEG by the radical polymerization method.

3.2 **Investigations of the thermal properties**

The thermal properties of p(DMAEMA-co-TPEG) were investigated from the second

DSC heating curves and cooling curves (**Figure 2**). The second DSC heating curves show an

obvious crystal melting transition over the lower temperature range, suggesting the formation

of a semi-crystalline soft phase based on the TPEG segments because the crystal melting

temperature (T_m) of p(DMAEMA-co-TPEG) is close to that of the pure TPEG, ca 55.5℃. As

the TPEG content increases, the T_m shifts to a higher temperature, and the enthalpy (ΔH)

significantly increases, suggesting the enhancement of crystallinity for the TPEG soft phase

(**Table S1**). The cooling curve also shows the formation of TPEG crystals. When the TPEG

content is higher than 40 wt%, an exothermic peak appears over the temperature range of

22.51 to 24.80℃, while another exothermic peak was detected at approximately 18.12℃ in

the TPEG40 and TPEG50 samples. When the TPEG content is lower than 30 wt%,

p(DMAEMA-co-TPEG) shows only one exothermic peak, implying that the TPEG segment

tends to congregate into the crystalline phase in the higher TPEG content samples, while the

congregation of the TPEG segment may be destroyed by the DMAEMA segment in the lower

TPEG content samples. Therefore, the crystallization of the dispersed TPEG segment requires

a lower crystalline temperature. This DSC result also demonstrates a possible changing

tendency of the TPEG phase from the dispersed semi-crystalline phase to a continuous
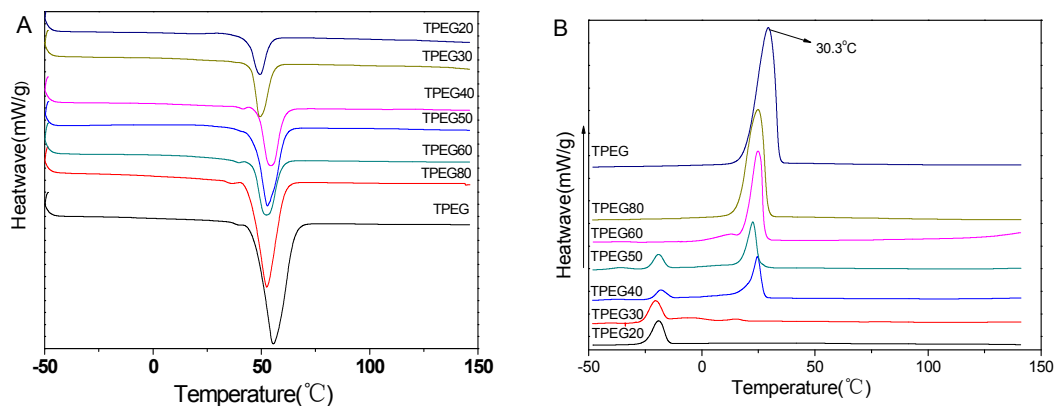
semi-crystalline phase.

Figure 2. DSC curves of p(DMAEMA-co-TPEG) (A-the second heating curves; B-the cooling curves)
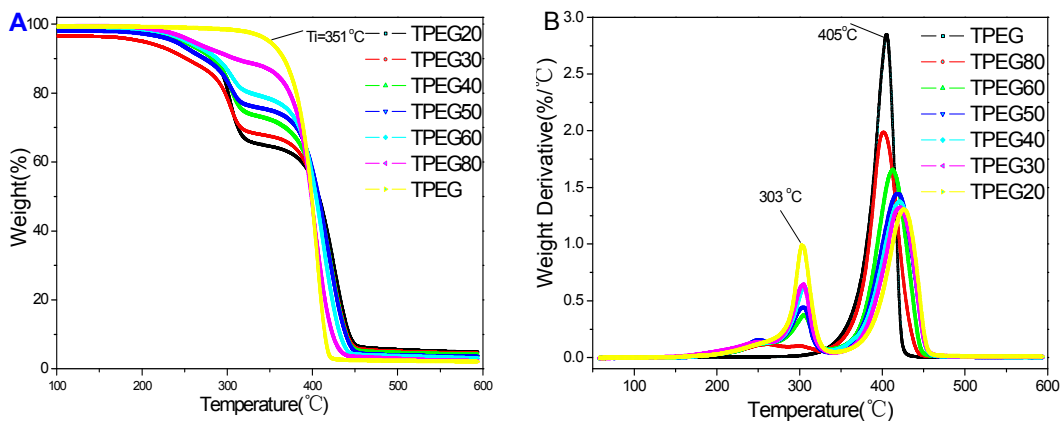

Figure 3.TG (A) and DTG (B) curves of p(DMAEMA-co-TPEG)

In contrast to the previous PEG derivatives based on methacrylate, TPEG tends to improve the thermal stability of p(DMAEMA-co-TPEG). The TG curves demonstrate that the initial decomposition temperature (T_i) for pure TPEG is higher than 351℃ because TPEG contains only ether groups as shown in the FT-IR spectrum (**Figure 1A**). The p(DMAEMA-co-TPEG) shows two stages of thermo-decomposition. The DMAEMA segment may start its decomposition below 257℃. As the TPEG content increases, the T_i shifts to a higher temperature, and the weight loss at the first stage significantly decreases, suggesting the enhancement of thermal stability at the first stages by the TPEG segment (**Figure 3A**). The DTG curves further show two peaks corresponding to the maximum decomposition temperatures, 303℃ for the DMAEMA segments and 405℃ for TPEG

10

segments, and the backbone in the entire p(DMAEMA-co-TPEG) (**Figure 3B**). Thus, it is confirmed that the TPEG block and the DMAEMA block are formed in the p(DMAEMA-co-TPEG).

Dynamic mechanical properties
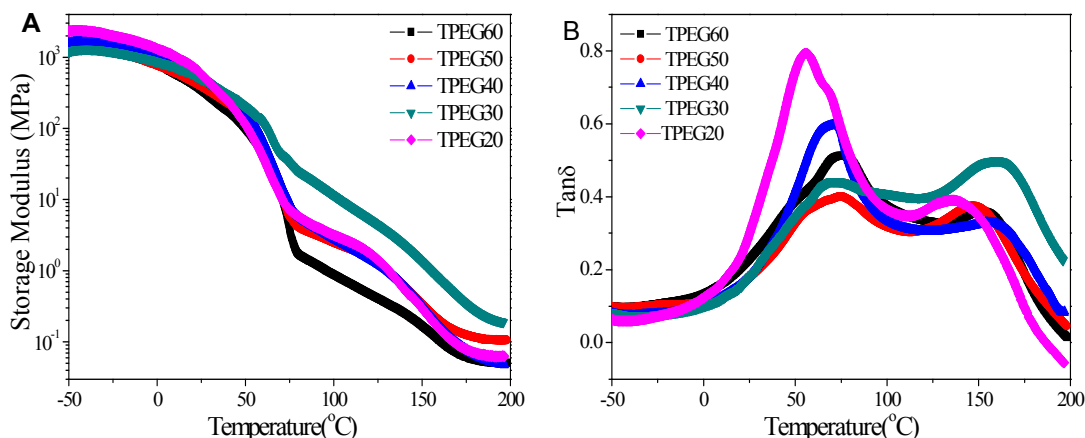
Figure 4. DMA curves of p(DMAEMA-co-TPEG)

The DMA curves provide another proof for the morphology of p(DMAEMA-co-TPEG). Figure 4A demonstrates that there is a large difference in the modulus up to a factor of 600 over the temperature range of 25 to 80℃, which is over the temperature range of crystal melting of TPEG as discussed in the DSC (**Figure 2A**). This result indicates that the modulus decrease should be ascribed to the crystal melting transition of the TPEG soft phase. Actually, the storage modulus starts to decrease at about -40℃. This earlier modulus decrease suggests that there is another weak glass transition in TPEG soft phase though the glass transition temperature (T_g) can not be detected on DSC curves. When the TPEG content decreases to below 40 wt%, another significant decrease in the storage modulus occurs over a higher temperature range from 125 to 175℃. Tanδ curves further show two large peaks corresponding to the chain movements of the two segments. The first peak is resulted from the crystal melting transition of TPEG segments. The second peak should be ascribed to the glass transition of DMAEMA segments since no crystal melting peaks are detected within this temperature range on DSC curves. These results suggest the formation of a soft phase-hard phase separation morphology in the p(DMAEMA-co-TPEG). In previous studies[58-60], many types of shape memory polymers have shown a similar phase separation structure composed of a soft phase and hard phase. The significant decrease of the modulus

11

during the crystal melting transition provides the possible structure to achieve good shape fixity, while the hard phase can provide physical netpoints to the shape recovery. Thus, it is expected that p(DMAEMA-co-TPEG) can be used as shape memory materials.
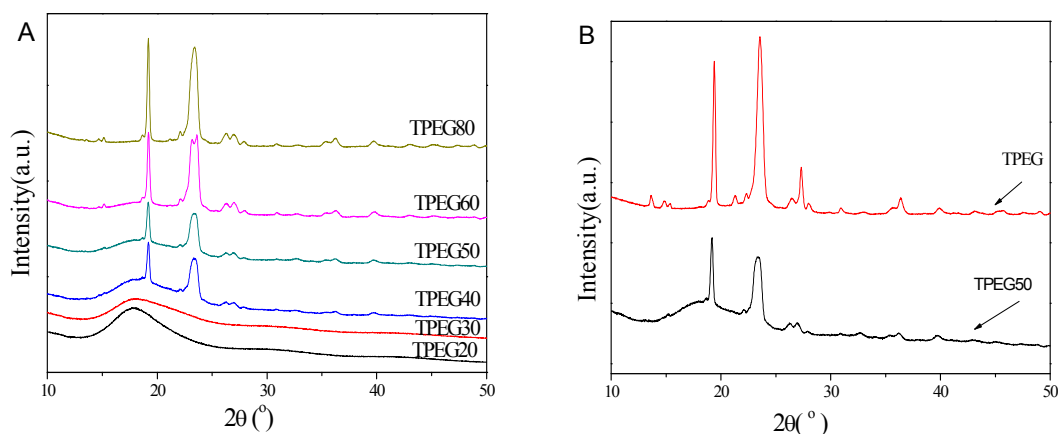
Morphology Analysis

Figure 5. XRD profiles of p(DMAEMA-co-TPEG) (A- for samples with different TPEG content; B-for comparison with pure TPEG)

Because TPEG might serve as a novel reversible phase for shape memory polymers, the crystallization behaviour of p(DMAEMA-co-TPEG) was further investigated using XRD, SEM and POM. Figure 5 presents the XRD patterns of p(DMAEMA-co-TPEG) with various TPEG contents. The XRD patterns demonstrate that p(DMAEMA-co-TPEG) have two prominent peaks at 2θ of 19.10° and 23.42° when the TPEG content is higher than 40 wt%, corresponding to the crystalline peaks of the TPEG segments because they are also detected in the pure TPEG (**Figure 5B**). Moreover, it is found that the peak density significantly decreases as the TPEG content decreases. Thus, it is confirmed that the crystalline structure stems from the TPEG soft segment, and the crystallinity of the TPEG soft segment is influenced by the TPEG content or DMAEMA content. This result is consistent with the DSC observation. Additionally, the TPEG20 and TPEG30 samples show no crystalline peaks because their crystallization requires a lower temperature as discussed in the DSC analysis.
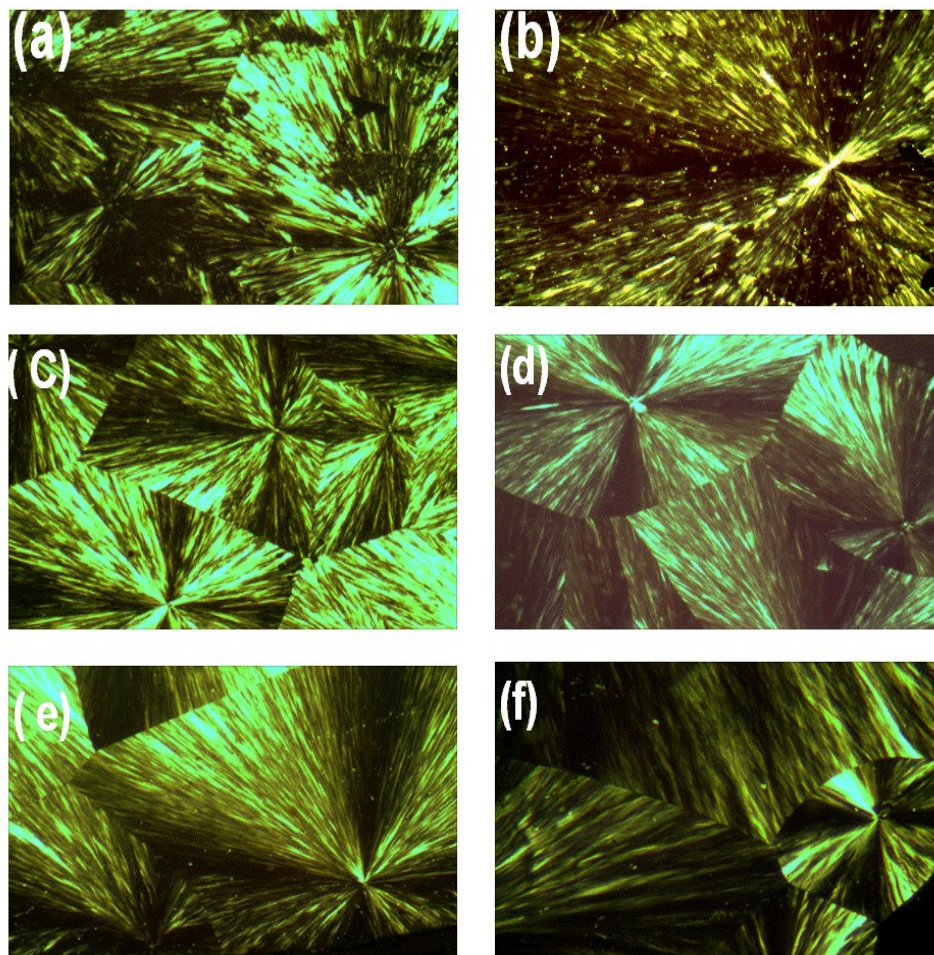
Figure 6. POM images of p(DMAEMA-co-TPEG) with different TPEG contents (a-TPEG80; b-TPEG60; c-TPEG50; d-TPEG40; e-TPEG30; and f-TPEG20)

The POM images provide visual proof for the crystallization of the TPEG soft segment. Figure 6 demonstrates that all of the p(DMAEMA-co-TPEG) have many "+" polarising optical patterns designated as spherical crystals.[58] During the experiment, it was also observed that the "+" polarising optical patterns appeared immediately in the pure TPEG after cooling to room temperature. As the TPEG content decreases, the formation of crystals requires more time in the p(DMAEMA-co-TPEG). Particularly, the TPEG20 and TPEG30 samples require more than 12 h at 20℃. These observations are consistent with the results of DSC and XRD. Thus, it is confirmed again that all of the spherical crystals result from the crystallization of the TPEG soft segment, and the crystallization rate is influenced by the DMAEMA segment.
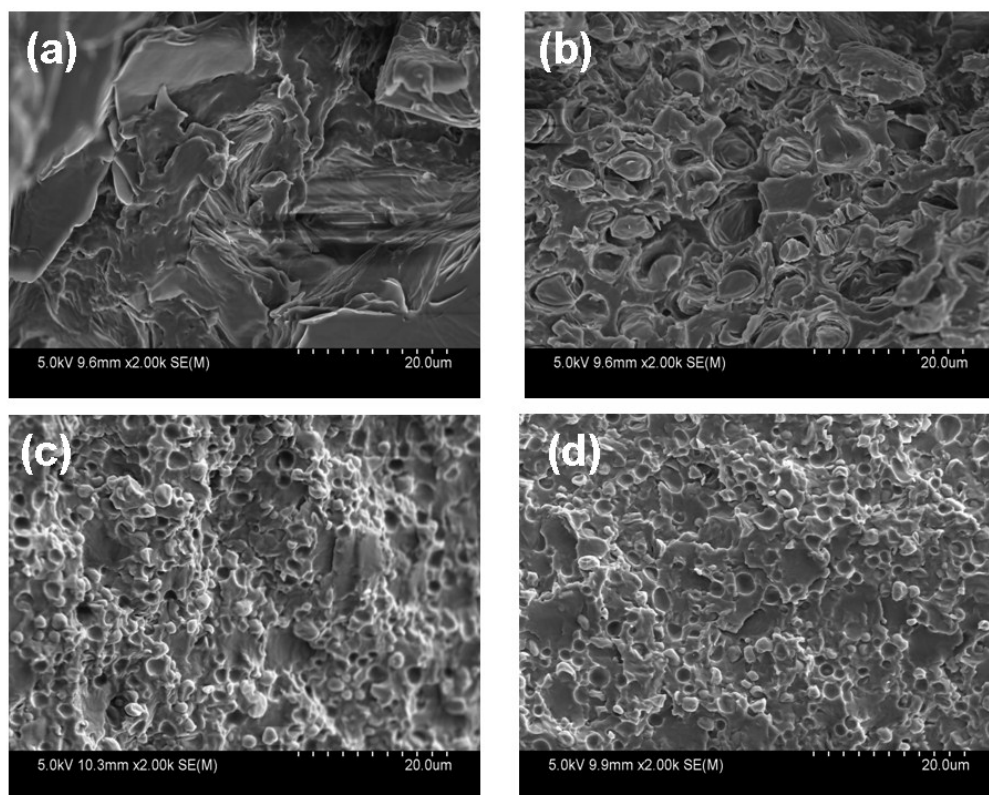
Figure 7. SEM images of p(DMAEMA-co-TPEG) with different TPEG contents

(a-TPEG60; b-TPEG50; c-TPEG30; and d-TPEG20)

The spherical crystals of the TPEG soft phase can also be observed in the SEM images. Figure 7 demonstrates that many spherical holes appear on the broken surface of p(DMAEMA-co-TPEG), confirming the formation of spherical crystals. As the TPEG content decreases, the size of the spherical holes decreases. In the high TPEG content copolymer, the spherical crystals tend to impinge on each other, suggesting the formation of a continuous TPEG crystalline phase. The spherical crystals are dispersed over another amorphous phase in the TPEG20 and TPEG30 samples, suggesting the formation of a dispersed TPEG phase. Thus, an illustration is proposed to explain the morphology change of p(DMAEMA-co-TPEG) by adjusting the TPEG content (**Figure 8**). The TPEG segments have good crystallizability. As the TPEG content increases, the morphology of the TPEG phase changes from dispersed small spherical crystals to a continuous crystalline phase composed of larger spherical crystals. This changing tendency is also reflected in the AFM images **(Figure S2)**. The dispersed TPEG crystals are reflected by small outshoots in the low TPEG-containing copolymer (**Figure S2-a,b**), whereas a continuous TPEG crystalline phase

14

is reflected by a "mountain chain" in the high TPEG-containing copolymers (**Figure S2-c,d**). Thus, p(DMAEMA-co-TPEG) with an excessively higher TPEG content could not form integrated smooth polymeric membranes due to its substantially higher crystallinity.
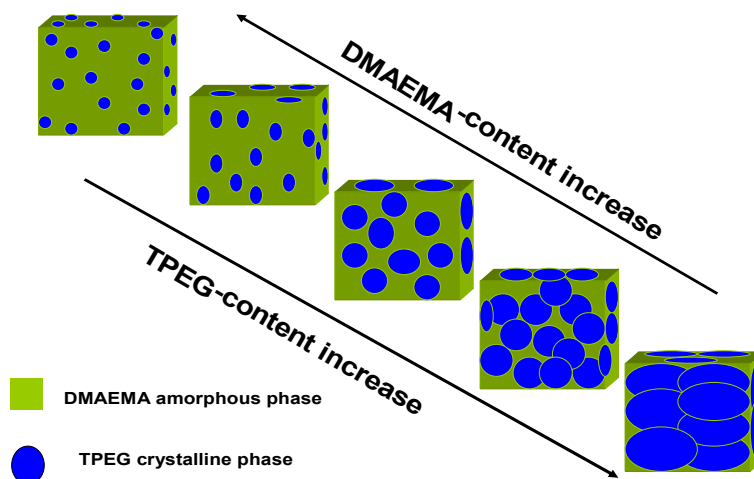

Figure 8. Illustration of the changing morphology as the TPEG content is adjusted in p(DMAEMA-co-TPEG)

Isothermal Crystallization Kinetics

To understand the role of TPEG crystals in the morphology of p(DMAEMA-co-TPEG), isothermal crystallization is fixed at 30℃ because the crystallization temperature of pure TPEG is approximately 30.3℃ on the DSC cooling curves (**Figure 2B**). Figure 9 presents the isothermal crystallization curves of p(DMAEMA-co-TPEG) with various TPEG contents. The exothermic curves demonstrate that the maximum exothermic peak was determined within 3 min in pure TPEG and in the TPEG80 sample (**Figure 9A**). As the TPEG content decreases from 80 to 40 wt%, the determined time increases, suggesting the slower crystallization speed in the lower TPEG-containing p(DMAEMA-co-TPEG). Similarly, no heat flow can be detected in the TPEG20 and TPEG30 samples due to their lower crystallization temperature and slow crystallization speed at 30℃. These observations are consistent with the POM results. The kinetics of the isothermal crystallization of the TPEG segment can be further analyzed with the Avrami equation, which is widely accepted to describe a variety of crystallization processes.[55] Relative crystallinity (X_t) was calculated based on the exothermic peak. Figure 9B demonstrates that X_t increases with the time of isothermal crystallization. A lower TPEG content indicates a lower crystallization rate. Using

the Ozawa equation (2) or equation (3), plots of log{-ln[1-X(t)]} against log t are presented in Figure 9C. From the plots, using equations (3) and (4), various parameters for isothermal crystallization kinetics, including n, logK, K and E, could be calculated (**Table S2**). Using equation (4), K and logK calculated based on t(0.5) matched well with those based on X(t). Thus, it is confirmed that the crystallization rate significantly decreases with the decrease of TPEG content; p(DMAEMA-co-TPEG) samples with higher TPEG contents show better crystallizability.
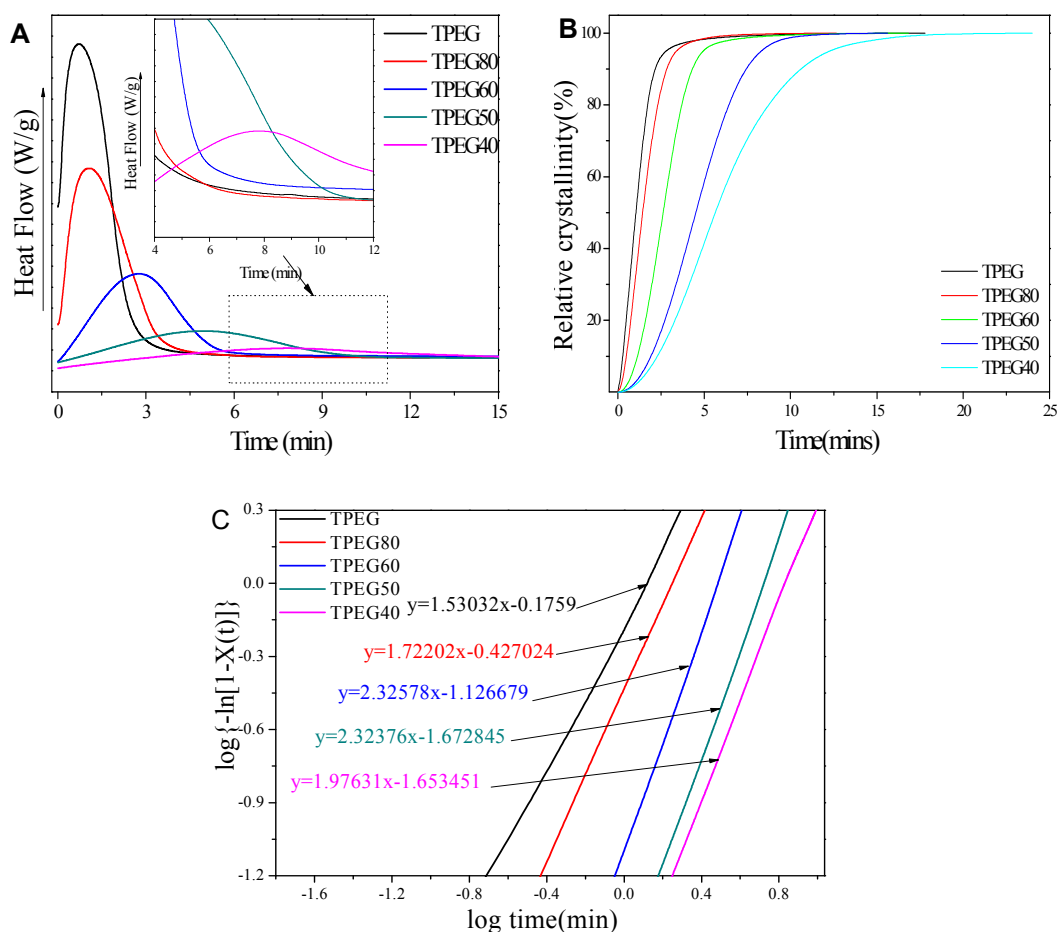
Figure 9. Isothermal crystallization of p(DMAEMA-co-TPEG): (A- exothermic curve versus time; B-dependency of relative crystallinity versus time; C- Plots of log{-ln[1-X(t)]} versus log t at 30℃)

Shape memory properties
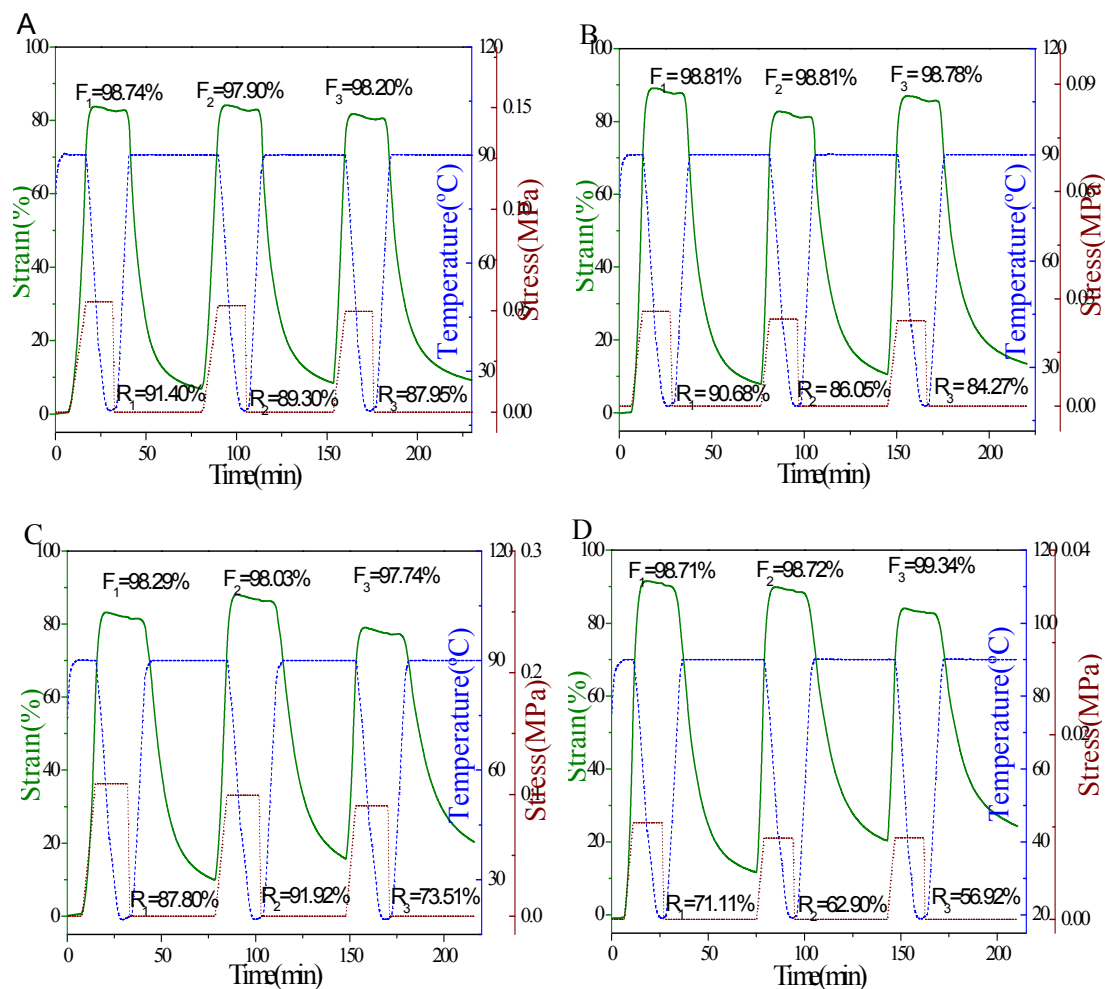
Figure 10. Thermal-mechanical curves showing repeated dual-shape memory cycle with the deformation and recovery temperature of 90℃ for p(DMAEMA-co-TPEG) with different TPEG contents: (A-TPEG50; B-TPEG40; C-TPEG30; and D-TPEG20)

The thermal-induced shape memory effect was investigated using DMA under the control force mode.[54] Figure 10 shows the obtained data proving the dual-shape memory effect. Sample TPEG50 could be deformed to approximately 83.64% strain when the sample was heated to 90°C, and more than 98.74% strain was fixed after cooling below 20°C. More than 91.4% strain recovery occurs when reheating to the deformation temperature (T_d) (**Figure 10A**), which is typical dual-shape memory behaviour. Moreover, this dual-shape memory effect can be repeated. The good shape fixity can be maintained over many cycles because of the good crystallinity of the sample as discussed above, whereas the shape recovery tends to decrease with time due to the destruction of the physical interactive

networks. Samples with more than 60 wt% TPEG content tend to show no dual-shape memory effect because they are too fragile to be deformed owing to their substantially higher crystallinity. The other samples also show similar dual-shape memory behaviour **(Figure 10B-C)**. Overall, as the TPEG content decreases, the shape recovery clearly decreases. The possible reason for this result is that a large fraction of the DMAEMA segments forms a continuous amorphous phase, but only a part of these segments provides physical interactive networks for shape recovery, while TPEG crystals are dispersed over the DMAEMA amorphous phase when the TPEG content is low (**see Figure 8**). Higher deformation at a higher temperature may also destroy the physical interactive networks because chain movement of the DMAEMA segments starts at approximately 90℃ as shown in the Tanδ curves (**Figure 4B**). The multi-shape memory effect might prove this hypothesis. Figure 11 presents the thermal-mechanical curves showing multi-shape memory cycles for sample TPEG20. The triple-shape memory cycle demonstrates that shape fixity at T_d=70℃ is higher than 70%, although no TPEG crystals are formed at this temperature. Shape fixity at T_d=20℃ is higher than 99% after the second deformation. During the recovery process, more than 104% of the deformed strain is recovered at the first stage (recovery temperature, T_r=70℃). Another 33.3% of strain can be further recovered by increasing the T_r to 110℃. This triple-shape memory effect is also good because the total shape recovery is higher than 92.6% (**Figure 11A**). The photos showing the triple-shape memory process also confirm that copolymer can fix two temporary shapes at 70℃ and 20℃, and recover them at 70℃ and 110℃ upon heating (see Figure S3). Multi-staged shape recovery also demonstrates that the deformed strain recovers from 85.58% to 36.69 at the first stage (T_r=70℃) and recovers to 10.76% at the second stage (T_r=90℃). Finally, another 4.85% of strain recovery requires a higher T_r of 110℃ (**Figure 11B**). Thus, it is confirmed that the shape memory mechanism of p(DMAEMA-co-TPEG) is ascribed to the strain fixing of the TPEG crystalline phase and the physical interactive networks of the DMAEMA segments. Compared with previous reports[1, 54, 61], p(DMAEMA-co-TPEG) copolymers are novel multi-shape memory polymers that can be further betainized to zwitterionic polymers for many biological applications.[7-12]
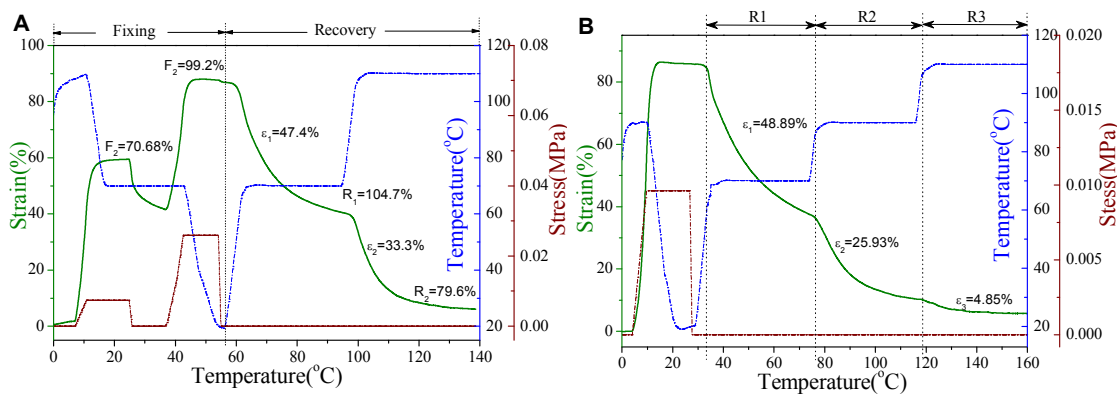
Figure 11．Thermal-mechanical curves showing multi-shape memory cycle for sample TPEG20 (A-triple-shape memory cycle with the deformation and recovery temperature of 110+70℃; B-multi-staged shape recovery with recovery temperature of 70+90+110℃ after one-step deformation at 110℃)
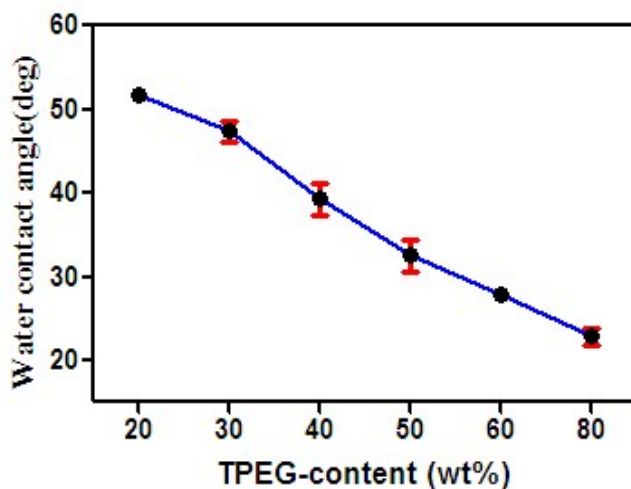

Figure 12. The dependency of water contact angle on TPEG content showing the hydrophilic properties of p(DMAEMA-co-TPEG)

PEG-based shape memory polymers have been widely used in biomedical applications because they show good biocompatibility due to their good hydrophilic properties. Considering the potential biological applications, the hydrophilic properties of p(DMAEMA-co-TPEG) were investigated from their water contact angles (**Figure 12**). Figure 12 demonstrates that all samples show a low water contact angle, suggesting good hydrophilic properties of p(DMAEMA-co-TPEG). Moreover, the water contact angle

decreases linearly from 51.63°to 22.83° as the TPEG content increases from 20 wt% to 80 wt%, suggesting better hydrophilicity in higher TPEG-containing p(DMAEMA-co-TPEG) **(Figure 12B)**. Although biocompatibility will be investigated in the following study, we believe that p(DMAEMA-co-TPEG) also has good biocompatibility due to their good hydrophilicity. Thus, these polymers show great promise for applications in the biomedical field, such as smart bandages, surgical sutures and gene or drug delivery.

Conclusions

In summary, we developed a novel shape memory copolymer based on TPEG and DMAEMA for potential biological applications. In these DMAEMA-TPEG copolymers, TPEG segments form a semi-crystalline phase that serves as the reversible phase, while DMAEMA segments form an amorphous phase containing physical interactive networks that serves as the hard phase. The TPEG segments exhibit good crystallizability, forming spherical crystals. As the TPEG content increases, crystallinity and the rate of crystallization increase, and the TPEG phase changes from dispersed small spherical crystals to a continuous crystalline phase. Additionally, good crystallinity of the TPEG phase endows the copolymers with good shape fixity, whereas the shape recovery decreases as the TPEG content decreases due to damage of the physical interactive networks. DMAEMA-TPEG copolymers also show the multi-shape memory effect with a good triple-shape memory effect. Finally, the investigation of the water contact angle also illustrates that all of the DMAEMA-TPEG copolymers have good hydrophilicity.

Electronic Supplementary Information (ESI) available:

Test 1: Shape Memory Behavior Testing

Figure S1. ATR-FTIR spectra of p(DMAEMA-co-TPEG) with different TPEG-content

Figure S2.AFM 3D-images of p(DMAEMA-co-TPEG) with different TPEG-content：
(a-TPEG20; b-TPEG50; c-TPEG60; d-TPEG80)

Table S1. DSC results of p(DMAEMA-co-TPEG)

Table S2. Parameters for isothermal crystallization kinetics at 30°C

Notes and References

1.   T. Xie, *Nature*, 2010, **464**, 267-270.

2.   R. Dolog and R. A. Weiss, *Macromolecules*, 2013, **46**, 7845-7852.

3.   A. M. Gumel and M. S. M. Annuar, *J.Appl. Polym.Sci.*, 2014, **131**.

4.   J. Dong, J. Ding, J. Weng and L. Dai, *Macromol. Rapid Comm.*, 2013, **34**, 659-664.

5.   L. Xian Kai, C. Li, Z. Yi Ping and D. Zhi Zhi, *J. Membrane Sci.*, 2010, **45**, 2703-2707.

6.   X. L. Zhu, Y. R. Gu, G. J. Chen, Z. P. Cheng and J. M. Lu, *J.Appl. Polym.Sci.*, 2004, **93**, 1539-1545.

7.   L.-J. Zhu, F. Liu, X.-M. Yu, A.-L. Gao and L.-X. Xue, *J. Membrane Sci.*, 2015, **475**, 469-479.

8.   S.-B. Yeh, C.-S. Chen, W.-Y. Chen and C.-J. Huang, *Langmuir*, 2014, **30**, 11386-11393.

9.   Y. Li, R. Liu, J. Yang, G. Ma, Z. Zhang and X. Zhang, *Biomaterials*, 2014, **35**, 9731-9745.

10.   L. Cheng, Y. Li, X. Zhai, B. Xu, Z. Cao and W. Liu, *ACS Appl. Mater. Inter.*, 2014, **6**, 20487-20497.

11.   A. Laschewsky, *Polymers*, 2014, **6**, 1544-1601.

12.   A. B. Lowe and C. L. McCormick, *Chem. Rev.*, 2002, **102**, 4177-4189.

13.   X. Wang, G. Jiang, Y. Wang, R. Wang, X. Sun, R. Hu, X. Xi, Y. Zhou, S. Wang and T. Wang, *J. Macromol. Sci. A*, 2013, **50**, 644-652.

14.   C. Wang, C. Ma, C. Mu and W. Lin, *Langmuir*, 2014, **30**, 12860-12867.

15.   C. Ma, H. Zhou, B. Wu and G. Zhang, *ACS Appl. Mater. Inter.*,, 2011, **3**, 455-461.

16.   T. Addison, O. J. Cayre, S. Biggs, S. P. Armes and D. York, *Langmuir*, 2010, **26**, 6281-6286.

17.   F. Taktak, M. Yildiz, H. Sert and C. Soykan, *J. Macromol. Sci. A*, 2015, **52**, 39-46.

18.   H. S. Lu, Z. Zhou, J. F. Jiang and Z. Y. Huang, *J.Appl. Polym.Sci.*, 2015, **132**, 8.

19.   J.-K. Y. Tan, J. L. Choi, H. Wei, J. G. Schellinger and S. H. Pun, *Biomater. Sci.*, 2015, **3**, 112-120.

20.   L. Carlsson, A. Fall, I. Chaduc, L. Wagberg, B. Charleux, E. Malmstrorn, F. D'Agosto, M. Lansalot and A. Carlmark, *Polym. Chem.-UK*, 2014, **5**, 6076-6086.

21.   Y.-Y. Yuan, C.-Q. Mao, X.-J. Du, J.-Z. Du, F. Wang and J. Wang, *Adv. Mater.*, 2012, **24**, 5476-5480.

22.   J.-T. Sun, Z.-Q. Yu, C.-Y. Hong and C.-Y. Pan, *Macromol. Rapid Comm.*, 2012, **33**, 811-818.

23.   G. Li, G. Cheng, H. Xue, S. Chen, F. Zhang and S. Jiang, *Biomaterials*, 2008, **29**, 4592-4597.

24.   Z. Zhang, S. Chen and S. Jiang, *Biomacromolecules*, 2006, **7**, 3311-3315.

25.   J. Gautier, E. Allard-Vannier, J. Burlaud-Gaillard, J. Domenech and I. Chourpa, *J.Biomed.Nanotechnol.*, 2015, **11**, 177-189.

26.   A. Patel, A. K. Gaharwar, G. Iviglia, H. Zhang, S. Mukundan, S. M. Mihaila, D. Demarchi and A. Khademhosseini, *Biomaterials*, 2013, **34**, 3970-3983.

27.   E. Moore, B. Delalat, R. Vasani, G. McPhee, H. Thissen and N. H. Voelcker, *ACS Appl. Mater. Inter.*, 2014, **6**, 15243-15252.

28.   J. Shi, L. Wang, J. Gao, Y. Liu, J. Zhang, R. Ma, R. Liu and Z. Zhang, *Biomaterials*, 2014, **35**, 5771-5784.

29.   L. Zhang, Y.-I. Jeong, S. Zheng, D. H. Kang, H. Suh and I. Kim, *Macromol. Biosci.*, 2014, **14**, 401-410.

30.   J. Wang, G. Yang, X. Guo, Z. Tang, Z. Zhong and S. Zhou, *Biomaterials*, 2014, **35**, 3080-3090.

31.   M. M. Porter, R. Imperio, M. Wen, M. A. Meyers and J. McKittrick, *Adv.Funct.Mater.*, 2014, **24**, 1978-1987.

RSC Advances Accepted Manuscript

32.   B. Ozcelik, A. Blencowe, J. Palmer, K. Ladewig, G. W. Stevens, K. M. Abberton, W. A. Morrison and G. G. Qiao, *Acta Biomater.*, 2014, **10**, 2769-2780.

33.   Y. Jiang, J. Chen, C. Deng, E. J. Suuronen and Z. Zhong, *Biomaterials*, 2014, **35**, 4969-4985.

34.   H. Y. Cho, S. E. Averick, E. Paredes, K. Wegner, A. Averick, S. Jurga, S. R. Das and K. Matyjaszewski, *Biomacromolecules*, 2013, **14**, 1262-1267.

35.   X. Z. Shu, Y. C. Liu, F. S. Palumbo, Y. Lu and G. D. Prestwich, *Biomaterials*, 2004, **25**, 1339-1348.

36.   A. Ovsianikov, M. Malinauskas, S. Schlie, B. Chichkov, S. Gittard, R. Narayan, M. Loebler, K. Sternberg, K. P. Schmitz and A. Haverich, *Acta Biomater.*, 2011, **7**, 967-974.

37.   X. Wei, G. Moad, B. W. Muir, E. Rizzardo, J. Rosselgong, W. Yang and S. H. Thang, *Macromol. Rapid Comm.*, 2014, **35**, 840-845.

38.   K. Wang, H. Peng, K. J. Thurecht, S. Puttick and A. K. Whittaker, *Polym.Chem.-UK*, 2014, **5**, 1760-1771.

39.   K. Sui, X. Shan, S. Gao, Y. Xia, Q. Zheng and D. Xie, *J. Polym. Sci.Polym. Chem.*, 2010, **48**, 2143-2153.

40.   X. J. Loh, S. J. Ong, Y. T. Tung and H. T. Choo, *Mat. Sci. Eng. C-Mater.*, 2013, **33**, 4545-4550.

41.   X. J. Loh, *J.Appl. Polym.Sci.*, 2013, **127**, 992-1000.

42.   C. Pietsch, U. Mansfeld, C. Guerrero-Sanchez, S. Hoeppener, A. Vollrath, M. Wagner, R. Hoogenboom, S. Saubern, S. H. Thang, C. R. Becer, J. Chiefari and U. S. Schubert, *Macromolecules*, 2012, **45**, 9292-9302.

43.   C. Cheng, A. J. Convertine, P. S. Stayton and J. D. Bryers, *Biomaterials*, 2012, **33**, 6868-6876.

44.   I. Javakhishvili, K. Jankova and S. Hvilsted, *Polym.Chem.-UK*, 2013, **4**, 662-668.

45.   D. Lin, Y. Huang, Q. Jiang, W. Zhang, X. Yue, S. Guo, P. Xiao, Q. Du, J. Xing, L. Deng, Z. Liang and A. Dong, *Biomaterials*, 2011, **32**, 8730-8742.

46.   A. Yasin, H. Li, Z. Lu, S. U. Rehman, M. Siddiq and H. Yang, *Soft Matter*, 2014, **10**, 972-977.

47.   Y. Feng, S. Zhang, L. Zhang, J. Guo and Y. Xu, *Polym. Adv. Technol.*, 2011, **22**, 2430-2438.

48.   A. B. Kutikov, K. A. Reyer and J. Song, *Macromol. Chem. Phys.*, 2014, **215**, 2482-2490.

49.   B. Guo, Y. Chen, Y. Lei, L. Zhang, W. Y. Zhou, A. B. M. Rabie and J. Zhao, *Biomacromolecules*, 2011, **12**, 1312-1321.

50.   C.S. Yang, H.C. Wu, J.S. Sun, H.M. Hsiao and T. W. Wang, *ACS Appl. Mater. Inter.*, 2013, **5**, 10985-10994.

51.   X. Yang, C. Cui, Z. Tong, C. R. Sabanayagam and X. Jia, *Acta Biomaterial.*, 2013, **9**, 8232-8244.

52.   W. Nan, W. Wang, H. Gao and W. Liu, *Soft Matter*, 2013, **9**, 132-137.

53.   E. Wornyo, K. Gall, F. Yang and W. King, *Polymer*, 2007, **48**, 3213-3225.

54.S. Chen, F. Mo, Y. Yang, F. J. Stadler, S. Chen, H. Yang and Z. Ge, *J.Mater.Chem. A*, 2015, **3**, 2924-2933.

55.   J. L. Hu, Y. Zhu, K. F. Choi, K. W. Yeung, Q. H. Meng and S. J. Chen, *J.Appl. Polym.Sci.*, 2008, **107**, 599-609.

56.   D. K. Wang, S. Varanasi, P. M. Fredericks, D. J. T. Hill, A. L. Symons, A. K. Whittaker and F. Rasoul, *J.Polym. Sci. Pol. Chem.*, 2013, **51**, 5163-5176.

57.   L. Yinwen, Y. Chaolong, Z. Yunfei, Z. Jian, G. Huilong and L. Mangeng, *Construction and Building Materials*, 2014, **64**, 324-332.

58.   S. J. Chen, J. L. Hu, Y. Q. Liu, H. M. Liem, Y. Zhu and Y. J. Liu, *J.Polym. Sci. Pol. Phys.*, 2007, **45**, 444-454.

59.   S. Chen, J. Hu, H. Zhuo and S. Chen, *J. Membrane Sci. ,* 2011, **46**, 5294-5304.

60.   F. Mo, F. Zhou, S. Chen, H. Yang, Z. Ge and S. Chen, *Polym. Int.,* 2014, DOI: 10.1002/pi.4814.

61.   L. Sun and W. M. Huang, *Soft Matter*, 2013, **6**, 4403-4406.

Notes:

aShenzhen Key Laboratory of Special Functional Materials, Nanshan District Key Lab for Biopolymers and Safety Evaluation, College of Materials Science and Engineering, Shenzhen

24

University, Shenzhen, 518060, China. [b]*College of Chemistry and Chemical Engineering, Shenzhen University, Shenzhen, 518060, China.*

*Corresponding author: College of Materials Science and Engineering，Shenzhen University, Shenzhen 518060, China. Tel and Fax: +86-755-26534562. E-mail: Shaojun Chen，chensj@szu.edu.cn Haitao Zhuo haitaozhuo@163.com

[&] Yangyang, Chen and Funian Mo are equal contributor to this work

RSC Advances Accepted Manuscript

Shape Memory Copolymer based on 2-(Dimethylamino) Ethyl Methacrylate and Methyl Allyl Polyethenoxy Ether for Potential Biological Applications

Yangyang, Chen[&a], Funian Mo[&a], Shaojun Chen[a], Yan Yang[a], Shiguo Chen[a]，Haitao Zhuo*[b], Jianhong Liu[b] ；*

[a]Shenzhen Key Laboratory of Special Functional Materials, Nanshan District Key Lab for Biopolymers and Safety Evaluation, College of Materials Science and Engineering, Shenzhen University, Shenzhen, 518060, China. [b]College of Chemistry and Chemical Engineering, Shenzhen University, Shenzhen, 518060, China.

*Corresponding author: College of Materials Science and Engineering，Shenzhen University, Shenzhen 518060, China. Tel and Fax: +86-755-26534562. E-mail: H.T.Zhuo haitaozhuo@163.com ; Shiguo Chen csg@szu.edu.cn

Graphical abstract